


Article

Angle Measurement of Objects outside the Linear Field of View of a Strapdown Semi-Active Laser Seeker

Yongbin Zheng * , Huimin Chen and Zongtan Zhou

College of Intelligence Science and Technology, National university of Defense Technology, Changsha 410073, China; fjxychm@163.com (H.C.); ztzhou@nudt.edu.cn (Z.Z.)

* Correspondence: zybnudt@nudt.edu.cn; Tel.: +86-731-8457-5322

Received: 25 March 2018; Accepted: 18 May 2018; Published: 23 May 2018



Abstract: The accurate angle measurement of objects outside the linear field of view (FOV) is a challenging task for a strapdown semi-active laser seeker and is not yet well resolved. Considering the fact that the strapdown semi-active laser seeker is equipped with GPS and an inertial navigation system (INS) on a missile, in this work, we present an angle measurement method based on the fusion of the seeker's data and GPS and INS data for a strapdown semi-active laser seeker. When an object is in the nonlinear FOV or outside the FOV, by solving the problems of space consistency and time consistency, the pitch angle and yaw angle of the object can be calculated via the fusion of the last valid angles measured by the seeker and the corresponding GPS and INS data. The numerical simulation results demonstrate the correctness and effectiveness of the proposed method.

Keywords: angle measurement for all-strapdown semi-active laser seeker; four-quadrant photoelectric detector; GPS and INS; data fusion; space consistency and time consistency

1. Introduction

Semi-active laser guidance, which has high precision and is easy to implement, is widely used in precision-guided weapons and equipment [1–4]. The core device is the semi-active laser seeker [5,6]. It receives the laser spot reflected by an object and detects the precise coordinates of the laser spot center by using a four-quadrant detector. It then calculates the pitch angle and the yaw angle between the object and the seeker's optical axis. However, a semi-active laser seeker cannot measure the angles when the object is out of the linear field of view (FOV) [7]. This problem is even worse for a strapdown semi-active laser seeker [8]. It is still one of the bottlenecks that restricts the overall application of strapdown semi-active laser seekers.

1.1. Detection Principle of the Strapdown Semi-Active Laser Seeker

The strapdown semi-active laser seeker is composed of a four-quadrant detector, optical system, circuit system and shell. The four-quadrant detector consists of four 90° photosensitive sectors with the same area and the same photoelectric response [9], which are represented by *I*, *II*, *III* and *IV*, respectively (as shown in Figure 1). Let *R* be the radius of the photosensitive surface, *r* be the radius of the reflected laser spot, (*x*, *y*) be the coordinates of the laser spot center and $I_{i(i=I,II,III,IV)}$ be the output current of the *i*-th photosensitive sectors, which is proportional to the energy of the received laser spot. There are three cases in which (*x*, *y*) can be detected using a four-quadrant detector. The first meets the condition $R < 2r < 2R$, that is the laser spot is located in the four-quadrant detector and covers each of the four photosensitive sectors (as shown in Figure 1). Then, (*x*, *y*) can be calculated by [10,11]:

$$\begin{cases} x = \frac{(I_I + I_{IV}) - (I_{II} + I_{III})}{I_I + I_{II} + I_{III} + I_{IV}} \\ y = \frac{(I_I + I_{II}) - (I_{III} + I_{IV})}{I_I + I_{II} + I_{III} + I_{IV}} \end{cases} \quad (1)$$

Obviously, $(x, y) = (0, 0)$ in the case shown in Figure 1a.

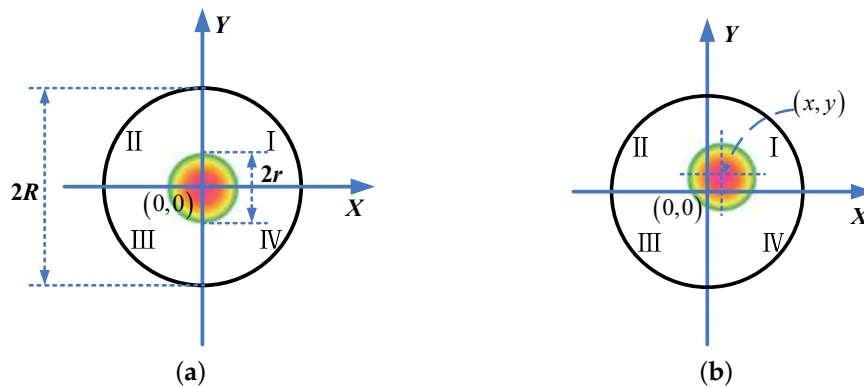


Figure 1. Detection principle of a four-quadrant detector. (a) The spot lies in the center; (b) The spot lies within the linear area.

The origin of the seeker's coordinate system is the origin of the four-quadrant detector, the seeker's X axis is along the optical axis of the optical system, and the seeker's Y and Z axes are along the Y and X axes of the four-quadrant detector, respectively. Based on (x, y) , the pitch angle ε and the yaw angle θ of the object relative to the seeker's coordinate system can be calculated using:

$$\varepsilon = \arctan\left(\frac{y}{f}\right), \theta = \arctan\left(\frac{x}{f}\right), \quad (2)$$

where f is the focal length of the seeker's optical system. In this case, the satisfied area on the four-quadrant detector is called the linear area of the detector, and the corresponding FOV of the seeker is called the linear FOV. The second case is when the laser spot is within the photosensitive surface of the four-quadrant detector, but it cannot cover all four quadrants of the photosensitive sector, as shown in Figure 2a. In this case, (x, y) cannot be precisely determined using Equation (1), and it can only be known in which quadrant the laser spot center is located. This area on the four-quadrant detector is called the nonlinear area, and the corresponding FOV of the seeker is called the nonlinear FOV. The third case is when the laser spot is outside the FOV of the semi-active laser seeker, as shown in Figure 2b. In this case, the four-quadrant detector cannot detect any information regarding the laser spot. Therefore, we must ensure that the object is within the linear FOV of the semi-active laser seeker.

1.2. Related Work

To ensure that the reflected laser spot lies in the linear area of the four-quadrant detector, the traditional semi-active laser seeker adopts a platform structure, that is the four-quadrant detector is installed on a complicated and high-precision servo control system [12]. The servo control system, which is composed of inertial measurement components and a dynamic follow-up system, can isolate the attitude movements of the seeker and ensure that the object is always located in the linear FOV of the seeker [4,13]. Although the platform-type semi-active laser seeker is a mature product, it has many disadvantages, such as a complex structure, high cost and large volume.

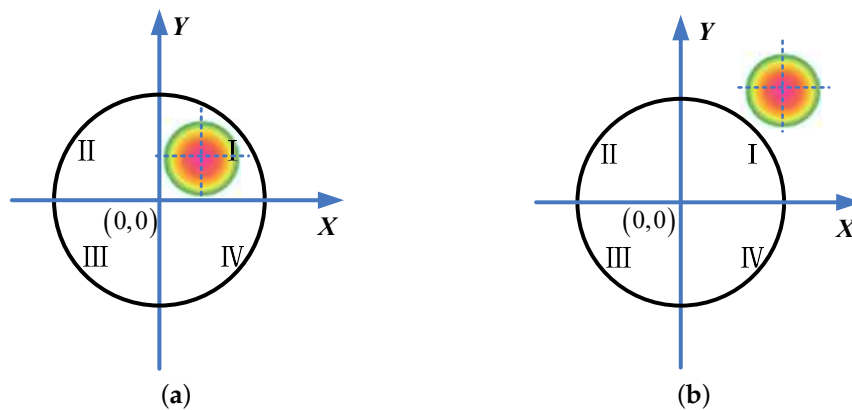


Figure 2. Examples of laser spot distribution on the four-quadrant detector. (a) The spot lies in the nonlinear area; (b) The spot is located outside the FOV.

In recent years, the strapdown semi-active laser seeker has become one of the main development directions of the semi-active seeker [14,15]. It removes the high-precision servo control system and places the four-quadrant detector directly onto the longitudinal axis of the seeker. The advantages are its simpler structure, higher reliability, smaller size, lighter weight and lower cost [16]. The main disadvantage is that due to the detector moving with the seeker, the problem of objects going outside the linear FOV is exacerbated. The current approach is to increase the linear FOV of the seeker via a special optics design [17–20]. However, there are three shortcomings to this approach. First, the amount by which the linear area of the detector can be expanded and the seeker FOV can be increased via optics design is very limited. Second, when the linear FOV increases, the angle measurement accuracy of the seeker will decrease, which will affect the guidance accuracy of the seeker [8]. Third, increasing the FOV of the seeker results in a shortening of the detection range, and the detection range is very important for the terminal guidance of a missile. Therefore, the problem of angle measurement for a strapdown laser seeker when objects are outside the linear FOV still hinders the full application of the strapdown semi-active laser seeker.

Considering the fact that the strapdown semi-active laser seeker is equipped with GPS and inertial attitude measurement equipment on the missile [21,22], in this work, we make full use of GPS and INS data and propose an angle measurement method for the strapdown semi-active laser seeker through data fusion.

2. Proposed Method

When an object is outside the linear FOV, by solving the space consistency problem and the time consistency problem, the pitch angle and the yaw angle can be calculated by fusing the following data: the current GPS and inertial attitude data, the angles measured by the seeker at the last moment when the object is in the linear FOV and the corresponding GPS and inertial attitude data at that moment. The following gives the specific details of this method.

2.1. Definition of Variables

Assume t_0 to be the last moment at which an object is located within the linear FOV of a strapdown semi-active laser seeker, and let the pitch angle and the yaw angle of the object measured by the seeker at t_0 be ε_0 and θ_0 , respectively. Suppose that at time t_1 , the object is outside the linear FOV of the seeker. Then, the pitch angle ε_1 and the yaw angle θ_1 cannot be measured by the seeker and will be calculated using the proposed method. Our method needs the following data: the object position O_T (longitude λ_T , latitude L_T and height h_T), which is given in advance; the position of the seeker at t_0 (longitude λ_0 , latitude L_0 and height h_0); the attitude data of the seeker with the yaw-pitch-roll rotation order at time t_0 (yaw angle φ_0 , pitch angle ψ_0 and roll angle γ_0) or the quaternions at t_0 (q_{0_0} , q_{1_0} , q_{2_0} , q_{3_0});

the position of the seeker at t_1 (longitude λ_1 , latitude L_1 and height h_1); and the attitude data of the seeker with the yaw-pitch-roll rotation order at time t_1 (yaw angle φ_1 , pitch angle ψ_1 and roll angle γ_1) or the quaternions at t_1 ($q_{0_1}, q_{1_1}, q_{2_1}, q_{3_1}$). The above positions and attitude data can be obtained via GPS and INS [23,24]. The problem of time consistency can be solved by precisely aligning the above data with the corresponding time.

2.2. Definitions of the Coordinate Systems

To solve the space consistency problem, we define the following coordinate systems.

The Earth-centered frame $O_e-X_eY_eZ_e$: The origin O_e is the center of the Earth. The axis O_eZ_e is perpendicular to the Earth's equatorial plane and points toward the North Pole. The axis O_eX_e lies in the Earth's equatorial plane and points to the Greenwich meridian. The axis O_eY_e is perpendicular to the plane $O_eX_eZ_e$ and forms a right-hand coordinate system with O_eX_e and O_eZ_e .

The local navigation frame $O_n-X_nY_nZ_n$: The local navigation frame is defined as having a north-up-east order. The origin O_n is the centroid of the seeker. The axis O_nY_n is collinear with the normal of the navigation frame's reference ellipsoid at the penetration point. The axis O_nX_n lies in the Meridian plane, is perpendicular to O_nY_n and points toward the north. The axis O_nZ_n is determined according to the right-hand rule.

The body frame $O_b-X_bY_bZ_b$: The origin O_b is the centroid of the seeker. The axis O_bX_b coincides with the longitudinal axis of the seeker and points toward the forward direction. The axis O_bY_b lies in the longitudinal symmetry plane of the seeker, is perpendicular to O_bX_b and points upward. The axis O_bZ_b is perpendicular to the $O_bX_bY_b$ plane and forms a right-hand coordinate system with O_bX_b and O_bY_b .

The on body line-of-sight frame $O_s-X_sY_sZ_s$: The origin O_s is the centroid of the seeker. O_sX_s points toward the object along the line of sight. The O_sY_s axis, which points upward, is on a plane that contains O_sX_s and is perpendicular to O_sX_s and the plane $O_bX_bZ_b$ at the same time. O_sZ_s is determined by the right-hand rule.

2.3. Analysis and Computation of the Proposed Method

In practice, the seeker moves with the missile all the time; thus, the position and attitude of the seeker at t_1 are different from those at t_0 . As shown in Figure 3, let O_{b0} be the seeker position at t_0 and $O_{b0}-X_{b0}Y_{b0}Z_{b0}$ be the body frame at O_{b0} . Moreover, let O_{b1} be the seeker position at t_1 and $O_{b1}-X_{b1}Y_{b1}Z_{b1}$ be the body frame at O_{b1} . From t_0 to t_1 , the body frame has both attitude movements and position movements simultaneously. Without loss of generality, we assume that the attitude movements occur first; the body frame $O_{b0}-X_{b0}Y_{b0}Z_{b0}$ transforms into the intermediate body frame $O_{b0}-X_{b1}Y_{b1}Z_{b1}$; and then, a translational movement occurs, with $O_{b0}-X_{b1}Y_{b1}Z_{b1}$ being translated to $O_{b1}-X_{b1}Y_{b1}Z_{b1}$. Therefore, the analysis and calculation required to solve the space consistency problem can be conducted in two stages.

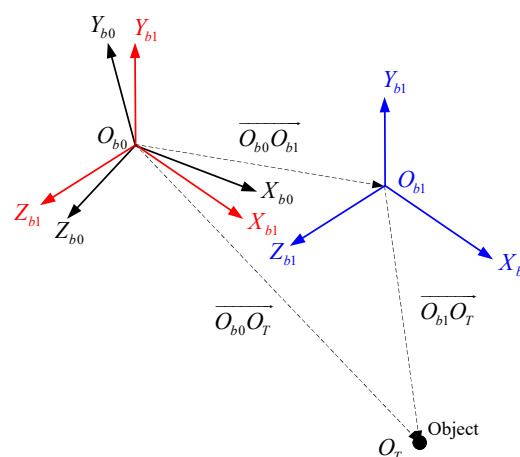


Figure 3. Equivalent decomposition of the seeker's movement from t_0 to t_1 .

2.3.1. First Stage of the Proposed Method

In the first stage, we consider only the variation of the pitch angle and the variation of the yaw angle caused by the seeker's attitude motion from t_0 to t_1 . In this stage, the pitch angle ε'_1 and yaw angle θ'_1 of the object should be calculated in the intermediate body frame $O_{b_0}-X_{b_1}Y_{b_1}Z_{b_1}$, with the calculation involving the following coordinate transformations: $O_{b_0}-X_{b_1}Y_{b_1}Z_{b_1}$ is transformed into the local navigation frame $O_n-X_nY_nZ_n$; then $O_n-X_nY_nZ_n$ is transformed into the body frame $O_{b_0}-X_{b_0}Y_{b_0}Z_{b_0}$; and finally, $O_{b_0}-X_{b_0}Y_{b_0}Z_{b_0}$ is transformed into the on body line-of-sight frame $O_s-X_sY_sZ_s$. The specific steps are as follows.

Step 1: $O_{b_0}-X_{b_1}Y_{b_1}Z_{b_1}$ is transformed into $O_n-X_nY_nZ_n$ by the roll-pitch-yaw rotation order with the rotations of $-\gamma_1$, $-\varphi_1$ and $-\psi_1$, respectively [25]. The transform matrix $C_{b_1}^{n0}$ is calculated according to Equation (3).

$$C_{b_1}^{n0} = \begin{bmatrix} \cos \psi_1 \cos \varphi_1 & -\cos \gamma_1 \sin \psi_1 \cos \varphi_1 + \sin \gamma_1 \sin \varphi_1 & \sin \gamma_1 \sin \psi_1 \cos \varphi_1 + \cos \gamma_1 \sin \varphi_1 \\ \sin \psi_1 & \cos \gamma_1 \cos \varphi_1 & -\sin \gamma_1 \cos \varphi_1 \\ -\cos \psi_1 \sin \varphi_1 & \cos \gamma_1 \sin \psi_1 \sin \varphi_1 + \sin \gamma_1 \cos \varphi_1 & -\sin \gamma_1 \sin \psi_1 \sin \varphi_1 + \cos \gamma_1 \cos \varphi_1 \end{bmatrix}. \quad (3)$$

To avoid the singularity problem of the Euler angles at about 90° , $C_{b_1}^{n0}$ can be calculated based on the quaternions $q_{0_1}, q_{1_1}, q_{2_1}, q_{3_1}$ according to Equation (4).

$$C_{b_1}^{n0} = \begin{bmatrix} q_{0_1}q_{0_1} + q_{1_1}q_{1_1} - q_{2_1}q_{2_1} - q_{3_1}q_{3_1} & 2(q_{1_1}q_{2_1} + q_{0_1}q_{3_1}) & 2(q_{1_1}q_{3_1} - q_{0_1}q_{2_1}) \\ 2(q_{1_1}q_{2_1} - q_{0_1}q_{3_1}) & q_{0_1}q_{0_1} - q_{1_1}q_{1_1} + q_{2_1}q_{2_1} - q_{3_1}q_{3_1} & 2(q_{2_1}q_{3_1} + q_{0_1}q_{1_1}) \\ 2(q_{1_1}q_{3_1} + q_{0_1}q_{2_1}) & 2(q_{2_1}q_{3_1} - q_{0_1}q_{1_1}) & q_{0_1}q_{0_1} - q_{1_1}q_{1_1} - q_{2_1}q_{2_1} + q_{3_1}q_{3_1} \end{bmatrix}. \quad (4)$$

Step 2: $O_n-X_nY_nZ_n$ is transformed into $O_{b_0}-X_{b_0}Y_{b_0}Z_{b_0}$ by the yaw-pitch-roll rotation order with rotations of ψ_0 , φ_0 and γ_0 , respectively. The transform matrix C_{n0}^{b0} is calculated according to Equation (5).

$$C_{n0}^{b0} = \begin{bmatrix} \cos \psi_0 \cos \varphi_0 & \sin \psi_0 & -\cos \psi_0 \sin \varphi_0 \\ -\cos \gamma_0 \sin \psi_0 \cos \varphi_0 + \sin \gamma_0 \sin \varphi_0 & \cos \gamma_0 \cos \varphi_0 & \cos \gamma_0 \sin \psi_0 \sin \varphi_0 + \sin \gamma_0 \cos \varphi_0 \\ \sin \gamma_0 \sin \psi_0 \cos \varphi_0 + \cos \gamma_0 \sin \varphi_0 & -\sin \gamma_0 \cos \varphi_0 & -\sin \gamma_0 \sin \psi_0 \sin \varphi_0 + \cos \gamma_0 \cos \varphi_0 \end{bmatrix}. \quad (5)$$

Similar to Step 1, C_{n0}^{b0} can be calculated based on the quaternions $q_{0_0}, q_{1_0}, q_{2_0}, q_{3_0}$ according to Equation (6):

$$C_{n0}^{b0} = \begin{bmatrix} q_{0_0}q_{0_0} + q_{1_0}q_{1_0} - q_{2_0}q_{2_0} - q_{3_0}q_{3_0} & 2(q_{1_0}q_{2_0} - q_{0_0}q_{3_0}) & 2(q_{1_0}q_{3_0} + q_{0_0}q_{2_0}) \\ 2(q_{1_0}q_{2_0} + q_{0_0}q_{3_0}) & q_{0_0}q_{0_0} - q_{1_0}q_{1_0} + q_{2_0}q_{2_0} - q_{3_0}q_{3_0} & 2(q_{2_0}q_{3_0} - q_{0_0}q_{1_0}) \\ 2(q_{1_0}q_{3_0} - q_{0_0}q_{2_0}) & 2(q_{2_0}q_{3_0} + q_{0_0}q_{1_0}) & q_{0_0}q_{0_0} - q_{1_0}q_{1_0} - q_{2_0}q_{2_0} + q_{3_0}q_{3_0} \end{bmatrix}. \quad (6)$$

Step 3: $O_{b_0}-X_{b_0}Y_{b_0}Z_{b_0}$ is transformed into $O_s-X_sY_sZ_s$ by the pitch-yaw rotation order with rotations of ε_0 and θ_0 . The transform matrix $C_{b_0}^s$ is:

$$C_{b_0}^s = \begin{bmatrix} \cos \theta_0 \cos \varepsilon_0 & \cos \theta_0 \sin \varepsilon_0 & -\sin \theta_0 \\ -\sin \varepsilon_0 & \cos \varepsilon_0 & 0 \\ \sin \theta_0 \cos \varepsilon_0 & \sin \theta_0 \sin \varepsilon_0 & \cos \theta_0 \end{bmatrix}. \quad (7)$$

To summarize, we can obtain the transformation matrix from $O_{b_0}-X_{b_1}Y_{b_1}Z_{b_1}$ to $O_s-X_sY_sZ_s$ as:

$$C_{b_0}^{s1} = C_{b_0}^s \cdot C_{n0}^{b0} \cdot C_{b_1}^{n0}. \quad (8)$$

Step 4: According to Equation (8), we can calculate the pitch angle ε'_1 using [25]:

$$\varepsilon'_1 = \begin{cases} \arctan\left(\frac{C_{b_0}^{S1}[1,2]}{C_{b_0}^{S1}[1,1]}\right), & \text{if } C_{b_0}^{S1}[1,2] \leq 0 \text{ and } C_{b_0}^{S1}[1,1] > -C_{b_0}^{S1}[1,2] \\ -\arctan\left(\frac{C_{b_0}^{S1}[1,1]}{C_{b_0}^{S1}[1,2]}\right) + \frac{\pi}{2}, & \text{if } C_{b_0}^{S1}[1,1] > 0 \text{ and } C_{b_0}^{S1}[1,1] \leq -C_{b_0}^{S1}[1,2] \\ -\arctan\left(\frac{C_{b_0}^{S1}[1,1]}{C_{b_0}^{S1}[1,2]}\right) - \frac{\pi}{2}, & \text{if } C_{b_0}^{S1}[1,1] \leq 0 \text{ and } C_{b_0}^{S1}[1,1] > C_{b_0}^{S1}[1,2] \\ \arctan\left(\frac{C_{b_0}^{S1}[1,2]}{C_{b_0}^{S1}[1,1]}\right) - \pi, & \text{if } C_{b_0}^{S1}[1,2] < 0 \text{ and } C_{b_0}^{S1}[1,1] \leq C_{b_0}^{S1}[1,2] \\ \arctan\left(\frac{C_{b_0}^{S1}[1,2]}{C_{b_0}^{S1}[1,1]}\right) + \pi, & \text{if } C_{b_0}^{S1}[1,2] \geq 0 \text{ and } -C_{b_0}^{S1}[1,1] > C_{b_0}^{S1}[1,2] \\ -\arctan\left(\frac{C_{b_0}^{S1}[1,1]}{C_{b_0}^{S1}[1,2]}\right) + \frac{\pi}{2}, & \text{if } C_{b_0}^{S1}[1,1] < 0 \text{ and } -C_{b_0}^{S1}[1,1] \leq C_{b_0}^{S1}[1,2] \\ -\arctan\left(\frac{C_{b_0}^{S1}[1,1]}{C_{b_0}^{S1}[1,2]}\right) + \frac{\pi}{2}, & \text{if } C_{b_0}^{S1}[1,1] \geq 0 \text{ and } C_{b_0}^{S1}[1,1] < C_{b_0}^{S1}[1,2] \\ \arctan\left(\frac{C_{b_0}^{S1}[1,2]}{C_{b_0}^{S1}[1,1]}\right), & \text{if } C_{b_0}^{S1}[1,2] > 0 \text{ and } C_{b_0}^{S1}[1,1] \geq C_{b_0}^{S1}[1,2] \end{cases}, \quad (9)$$

and the yaw angle θ'_1 using:

$$\theta'_1 = -\arcsin(C_{b_0}^{S1}[1,3]). \quad (10)$$

2.3.2. Second Stage of the Proposed Method

In the second stage, we analyze the variation of the pitch angle and the variation of the yaw angle caused by translating $O_{b_0}-X_{b_1}Y_{b_1}Z_{b_1}$ to $O_{b_1}-X_{b_1}Y_{b_1}Z_{b_1}$. As shown in Figure 3, to calculate the vector $\vec{O_{b_1}O_T}$, we first need to calculate the vector $\vec{O_{b_0}O_{b_1}}$ and the vector $\vec{O_{b_0}O_T}$ in frame $O_{b_0}-X_{b_1}Y_{b_1}Z_{b_1}$. The steps of calculating $\vec{O_{b_0}O_{b_1}}$ in $O_{b_0}-X_{b_1}Y_{b_1}Z_{b_1}$ are as follows.

Step 1: Calculate the radius R_{W0} of curvature in the prime vertical of the Earth and the radius R_{N0} of curvature in the meridian of the Earth at O_{b_0} by:

$$\begin{cases} R_{W0} = \frac{a_e^2}{(a_e^2 \cos^2 L_0 + b_e^2 \sin^2 L_0)^{1/2}}, \\ R_{N0} = R_{w0} \frac{b_e^2}{a_e^2} \end{cases}, \quad (11)$$

and calculate the radius R_{W1} of curvature in the prime vertical of the Earth and the radius R_{N1} of curvature in the meridian of the Earth at O_{b_1} by:

$$\begin{cases} R_{W1} = \frac{a_e^2}{(a_e^2 \cos^2 L_1 + b_e^2 \sin^2 L_1)^{1/2}}, \\ R_{N1} = R_{w1} \frac{b_e^2}{a_e^2} \end{cases}, \quad (12)$$

where $a_e = 6,378,140$ m and $b_e = a_e(1 - 1/298.257)$ are the lengths of the Earth's long and short half-axes, respectively.

Step 2: Calculate the coordinates $[e_{x0}, e_{y0}, e_{z0}]^T$ of O_{b_0} in the Earth-centered frame $O_e-X_eY_eZ_e$ using:

$$\begin{cases} e_{x0} = (R_{w0} + h_0) \cos L_0 \cos \lambda_0 \\ e_{y0} = (R_{w0} + h_0) \cos L_0 \sin \lambda_0, \\ e_{z0} = (R_{N0} + h_0) \sin L_0 \end{cases} \quad (13)$$

and the coordinates $[e_{x1}, e_{y1}, e_{z1}]^T$ of O_{b1} in $O_e-X_eY_eZ_e$ using:

$$\begin{cases} e_{x1} = (R_{W1} + h_1) \cos L_1 \cos \lambda_1 \\ e_{y1} = (R_{W1} + h_1) \cos L_1 \sin \lambda_1 \\ e_{z1} = (R_{W1} + h_1) \sin L_1 \end{cases} \quad (14)$$

Step 3: Calculate the transformation matrix C_e^{n0} from the Earth-centered frame $O_e-X_eY_eZ_e$ to the local navigation frame $O_n-X_nY_nZ_n$ at O_{b0} by:

$$C_e^{n0} = \begin{bmatrix} -\sin L_0 \cos \lambda_0 & -\sin L_0 \sin \lambda_0 & \cos L_0 \\ \cos L_0 \cos \lambda_0 & \cos L_0 \sin \lambda_0 & \sin L_0 \\ -\sin \lambda_0 & \cos \lambda_0 & 0 \end{bmatrix}. \quad (15)$$

Step 4: Calculate the transformation matrix C_{n0}^{b1} from the local navigation frame at O_{b0} to $O_{b0}-X_{b1}Y_{b1}Z_{b1}$ by:

$$C_{n0}^{b1} = (C_{b1}^{n0})^T. \quad (16)$$

From Step 1 to Step 4, $\overrightarrow{O_{b0}O_{b1}}$ can be obtained by:

$$\overrightarrow{O_{b0}O_{b1}} = C_{n0}^{b1} \cdot C_e^{n0} \cdot \begin{bmatrix} e_{x1} - e_{x0} \\ e_{y1} - e_{y0} \\ e_{z1} - e_{z0} \end{bmatrix}. \quad (17)$$

The vector $\overrightarrow{O_{b0}O_T}$ in frame $O_{b0}-X_{b0}Y_{b0}Z_{b0}$ is calculated as follows.

Step 1: Calculate the radius R_{WT} of curvature in the prime vertical of the Earth and the radius R_{NT} of curvature in the meridian of the Earth at the object position O_T by:

$$\begin{cases} R_{WT} = \frac{a_e^2}{(a_e^2 \cos^2 L_T + b_e^2 \sin^2 L_T)^{1/2}} \\ R_{NT} = R_{wT} \frac{b_e^2}{a_e^2} \end{cases} \quad (18)$$

Step 2: Calculate the coordinates $[e_{xT}, e_{yT}, e_{zT}]^T$ of O_T in the Earth-centered frame by:

$$\begin{cases} e_{xT} = (R_{wT} + h_T) \cos L_T \cos \lambda_T \\ e_{yT} = (R_{wT} + h_T) \cos L_T \sin \lambda_T \\ e_{zT} = (R_{NT} + h_T) \sin L_T \end{cases} \quad (19)$$

Step 3: Calculate the distance Dis_{t_0} between the seeker and the object at t_0 by:

$$Dis_{t_0} = \sqrt{(e_{x0} - e_{xT})^2 + (e_{y0} - e_{yT})^2 + (e_{z0} - e_{zT})^2}. \quad (20)$$

Step 4: Since the 3-2 order pitch angle and yaw angle of the object in $O_{b0}-X_{b1}Y_{b1}Z_{b1}$ are ϵ'_1 and θ'_1 , respectively, $\overrightarrow{O_{b0}O_T}$ is obtained by:

$$\overrightarrow{O_{b0}O_T} = \begin{bmatrix} Dis_{t_0} \cdot \cos \theta'_1 \cdot \cos \epsilon'_1 \\ Dis_{t_0} \cdot \cos \theta'_1 \cdot \sin \epsilon'_1 \\ -Dis_{t_0} \cdot \sin \theta'_1 \end{bmatrix}. \quad (21)$$

Step 5: The vector $\overrightarrow{O_{b1}O_T}$ is calculated using:

$$\overrightarrow{O_{b1}O_T} = \overrightarrow{O_{b0}O_T} - \overrightarrow{O_{b0}O_{b1}}. \tag{22}$$

Let the three components of $\overrightarrow{O_{b1}O_T}$ be $\Delta_{x_{f1}}$, $\Delta_{y_{f1}}$ and $\Delta_{z_{f1}}$; then, the pitch angle ε_1 and the yaw angle θ_1 of the object at time t_1 are finally determined as [25]:

$$\varepsilon_1 = \begin{cases} \arctan\left(\frac{\Delta_{y_{f1}}}{\Delta_{x_{f1}}}\right), & \text{if } \Delta_{y_{f1}} \leq 0 \text{ and } \Delta_{x_{f1}} > -\Delta_{y_{f1}} \\ -\arctan\left(\frac{\Delta_{x_{f1}}}{\Delta_{y_{f1}}}\right) - \frac{\pi}{2}, & \text{if } \Delta_{x_{f1}} > 0 \text{ and } \Delta_{x_{f1}} \leq -\Delta_{y_{f1}} \\ -\arctan\left(\frac{\Delta_{x_{f1}}}{\Delta_{y_{f1}}}\right) - \frac{\pi}{2}, & \text{if } \Delta_{x_{f1}} \leq 0 \text{ and } \Delta_{x_{f1}} > \Delta_{y_{f1}} \\ \arctan\left(\frac{\Delta_{y_{f1}}}{\Delta_{x_{f1}}}\right) - \pi, & \text{if } \Delta_{y_{f1}} < 0 \text{ and } \Delta_{x_{f1}} \leq \Delta_{y_{f1}} \\ \arctan\left(\frac{\Delta_{y_{f1}}}{\Delta_{x_{f1}}}\right) + \pi, & \text{if } \Delta_{y_{f1}} \geq 0 \text{ and } -\Delta_{x_{f1}} > \Delta_{y_{f1}} \\ -\arctan\left(\frac{\Delta_{x_{f1}}}{\Delta_{y_{f1}}}\right) + \frac{\pi}{2}, & \text{if } \Delta_{x_{f1}} < 0 \text{ and } -\Delta_{x_{f1}} \leq \Delta_{y_{f1}} \\ -\arctan\left(\frac{\Delta_{x_{f1}}}{\Delta_{y_{f1}}}\right) + \frac{\pi}{2}, & \text{if } \Delta_{x_{f1}} \geq 0 \text{ and } \Delta_{x_{f1}} < \Delta_{y_{f1}} \\ \arctan\left(\frac{\Delta_{y_{f1}}}{\Delta_{x_{f1}}}\right), & \text{if } \Delta_{y_{f1}} > 0 \text{ and } \Delta_{x_{f1}} \geq \Delta_{y_{f1}} \end{cases} \tag{23}$$

and:

$$\theta_1 = \arctan\left(\frac{\Delta_{z_{f1}}}{\sqrt{\Delta_{x_{f1}}^2 + \Delta_{y_{f1}}^2}}\right). \tag{24}$$

3. Numerical Simulation Results

3.1. Numerical Simulation Setups

We carry out two simulation experiments using MATLAB to verify and evaluate the proposed method. The setups of the simulations are as follows: the measurement period of the seeker is 50 ms; the linear FOV of the seeker is $\pm 10^\circ$; and the FOV of the seeker is $\pm 20^\circ$. In the simulations, the seeker performs a sinusoidal-like motion to place the object at different positions within the seeker’s FOV. As shown in Table 1, the object is in the linear FOV in the first frame, and the pitch angle and yaw angle are 6.752° and -7.187° , respectively. The object exits the linear FOV in the second frame (0.05 s) and stays in the nonlinear FOV from 0.05 s to 0.90 s. Then, the object leaves the FOV of the seeker at 0.95 s, re-enters the nonlinear FOV at 2.80 s and stays in the nonlinear FOV until 3.65 s. Next, it enters the linear FOV again and stays in the linear FOV until 5.05 s. Subsequently, the object again exits the linear FOV at 5.10 s and stays in the nonlinear FOV until 6.25 s. The object then stays outside the FOV between 6.30 s and 7.40 s before entering the nonlinear FOV at 7.45 s. In the simulations, we calculate the pitch angle and the yaw angle via the proposed method when the object exits the linear FOV of the seeker and evaluate the method’s performance by comparing it to the ground truth.

Table 1. Relationship between the object position and the seeker FOV.

| Time t (s) | 0 | 0.05–0.90 | 0.95–2.75 | 2.80–3.65 | 3.7–5.05 | 5.10–6.25 | 6.30–7.40 | 7.45–8.5 |
|--------------------------|--------|-----------|-----------|-----------|----------|-----------|-----------|-----------|
| Position relative to FOV | Linear | Nonlinear | Outside | Nonlinear | Linear | Nonlinear | Outside | Nonlinear |

3.2. Numerical Simulation Results

The purpose of the first numerical simulation is to verify the correctness of the proposed method. In the numerical simulation, the GPS and INS data do not contain errors. The results are shown in Figure 4. Figure 4a shows the pitch angle results, while Figure 4b shows the yaw angle results. The blue ‘o’ represents the ground truth, the red ‘+’ the result of the proposed method and the green ‘*’ the error between the proposed algorithm and the ground truth. It can be seen that both the pitch angle

errors and the yaw angle errors are very close to zero throughout the simulation. To be more precise, the absolute values of both the pitch angle errors and the yaw angle errors are less than 1×10^{-6} , which are caused by the numerical truncation of the simulation software. Therefore, this simulation result proves the correctness of the proposed method.

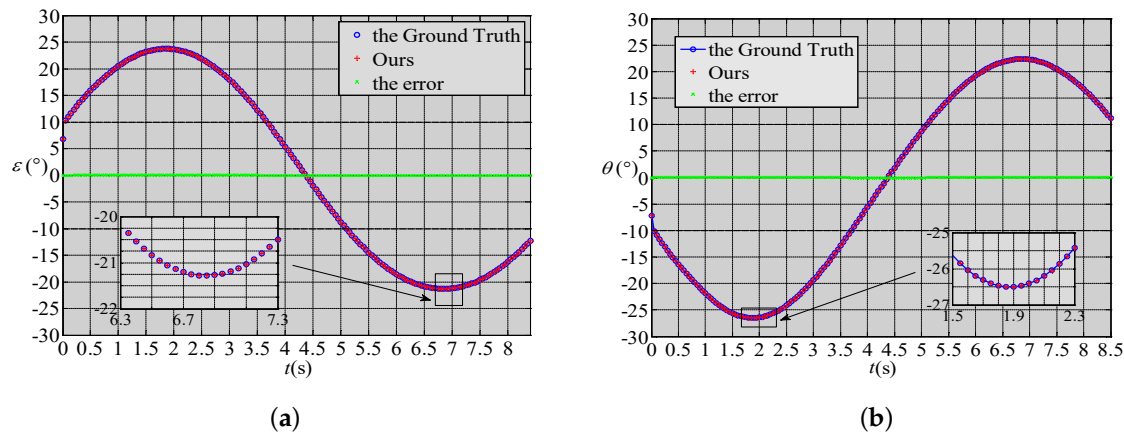


Figure 4. Results of the first numerical simulation. (a) The pitch angle results; (b) The yaw angle results.

The purpose of the second numerical simulation is to evaluate the angle measurement accuracy of the proposed method when the object is outside the linear FOV. In the numerical simulation, both the GPS data and INS data contain errors. The error in terms of the GPS latitude, longitude and height is 10 m. To make this numerical simulation more challenging, we assume that the INS uses a low-precision MEMS gyroscope [26,27] and that the angle drift ratio is $20^\circ/\text{h}$. In addition, we assume that the INS has been working for 60 s after the initial alignment. Thus, the initial attitude error of the INS is 0.333° . The attitude error of the INS during the numerical simulation is represented by the green curve in Figure 5c. The simulation results are shown in Figure 5: Figure 5a shows the pitch angle results; Figure 5b shows the yaw angle results; and Figure 5c shows the error between the proposed method and the ground truth. In Figure 5a,b, the blue curve represents the ground truth, while the red curve represents the result of the proposed method. In Figure 5c, the red '+' represents the pitch angle error, and the blue 'o' represents the yaw angle error. It can be seen that as time progresses, the object enters the nonlinear FOV or comes out of the FOV, and the angular measurement error of this method increases with the increase of the attitude error of the INS. Specifically, within the 3.6 s when the object leaves the linear FOV for the first time, as the attitude error of the INS increases to 0.354° , the absolute value of the pitch angle error of the proposed method increases from 0 to 0.14° , and the absolute value of the yaw angle error increases from 0 to 0.068° . Furthermore, we can conclude that under the above GPS and INS error conditions, this method can ensure that the angular measurement error is less than 0.2° in the 6.5 s when the object is outside the linear FOV.

From the theoretical derivation and simulation process, it can be seen that when the object is outside the linear FOV, the angle measurement accuracy of the method increases as the GPS accuracy and INS accuracy increase and as time reduces. In practice, the accuracy of the INS is higher than $20^\circ/\text{h}$, and the amount of time the object spends outside the linear FOV does not exceed 3.6 s. Thus, the proposed method can achieve better angle measurement performance than exhibited during the numerical simulation.

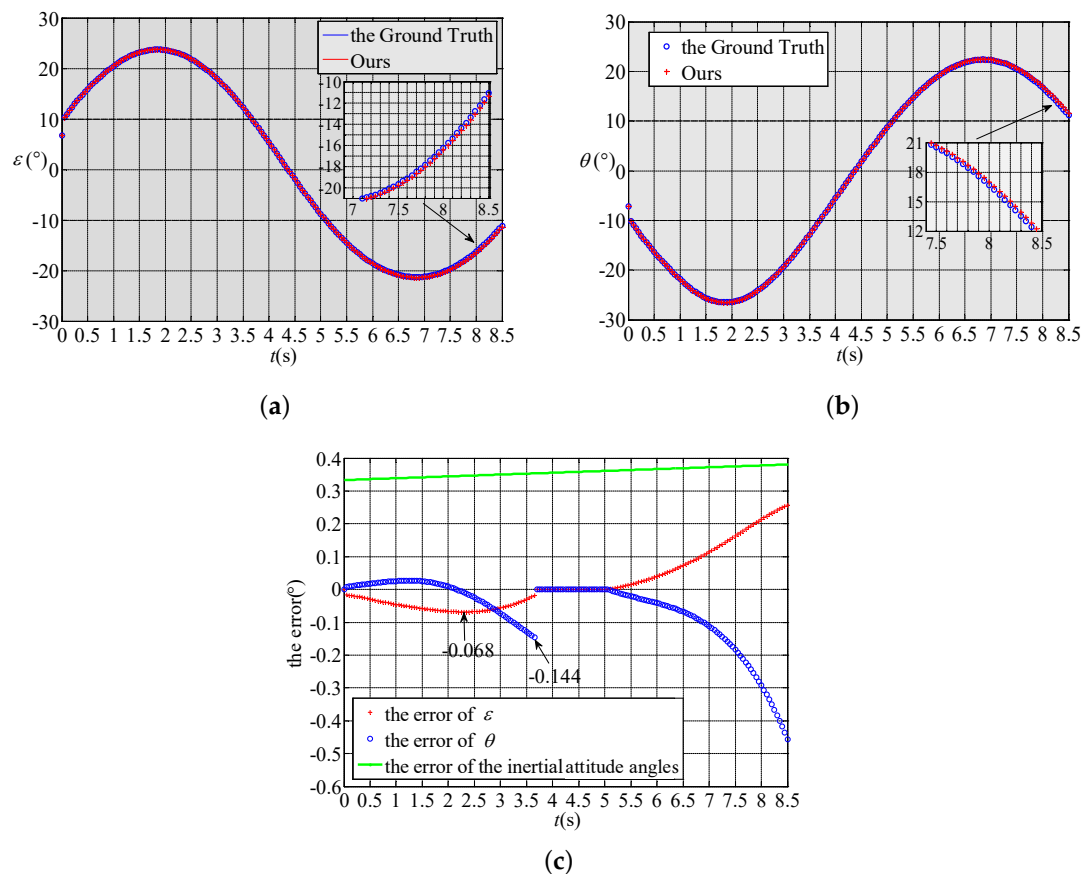


Figure 5. Results of the second numerical simulation. (a) The pitch angle results; (b) The yaw angle results; (c) The error between the proposed method and the ground truth.

4. Conclusions

To solve the problem in which a strapdown semi-active laser seeker cannot measure the angles of objects outside the linear FOV, we make full use of GPS and INS data and propose an angle measurement method based on information fusion. When an object is within the nonlinear FOV or outside the FOV, the pitch angle and the yaw angle of the object can be calculated via a fusion of the last valid angles measured by the seeker and the corresponding GPS and INS data. The numerical simulation results show that the proposed method can tolerate a certain amount of GPS and INS errors and ensure the angular measurement error is less than 0.2° in the 6.5 s when the object is outside the linear FOV. In general, the proposed method is simple, accurate and effective for angle measurement of objects outside the linear FOV of a strapdown semi-active laser seeker.

Author Contributions: Y.Z. proposed the method. Y.Z. and Z.Z. conceived of and designed the experiments. H.C. performed the experiments and helped perform the data analysis. Y.Z. wrote the paper. All the authors reviewed and approved the entire manuscript.

Funding: This work is supported by the National Natural Science Foundation of China (No. 61403412).

Conflicts of Interest: The authors declare no conflict of interest.

Abbreviations

The following abbreviations are used in this manuscript:

| | |
|------|---------------------------------|
| FOV | linear field of view |
| INS | inertial navigation system |
| MEMS | micro electromechanical systems |

References

1. Robert, A.N.; Harold, L. Copperhead Semiactive Laser Guidance System Development. *J. Guid. Control Dynam.* **1979**, *2*, 374–381, doi:10.2514/3.558927. [[CrossRef](#)]
2. Hubbard, K.; Katulka, G.; Lyon, D.; Petrick, D.; Fresconi, F.; Horwath, T. Low-Cost Semi-Active Laser Seekers for US Army Application. In Proceedings of the International Telemetering Conference, San Diego, CA, USA, 27–30 October 2008.
3. Allen, R.; Volpi, J.; Roemerman, S. COTS lens and detector characterization for low cost, miniature SAL seekers. In Proceedings of the Aiaa Guidance, Navigation, and Control Conference, Boston, MA, USA, 19–22 August 2013.
4. Titterton, D.H. *Military Laser Technology and Systems*; Artech House: Norwood, MA, USA, 2015.
5. English, J.E.; Pittman, W.C. Polarized Semi-Active Laser Last Pulse Logic Seeker Using a Staring Focal Plane Array. U.S. Patent 6,987,256, 17 January 2006.
6. Taylor, B.; Schaub, M.; Jenkins, D. Projectile Guidance System Including a Compact Semi-Active Laser Seeker. U.S. Patent 8,207,481, 26 June 2012.
7. Zhang, L.; Yang, Y.; Xia, W.; Zhu, X.; Chen, W.; Lu, Y. Linearity of quadrant avalanche photodiode in laser tracking system. *Chin. Opt. Lett.* **2009**, *7*, 728–731. [[CrossRef](#)]
8. Zhang, X.; Du, Z.Y.; Qiao, Y.F. Study on linear field of strapdown semi-active laser seeker. *Chin. Opt.* **2015**, *8*, 415–421. [[CrossRef](#)]
9. Zhang, H.; Chen, Y.S.; Geng, T.W.; Tao, C. Study on Main Factors Affecting Position Detection Accuracy of Four-Quadrant Detector. *Chin. J. Lasers* **2015**, *42*, 1217002. [[CrossRef](#)]
10. Tang, Y.; Gu, G.; Qian, W.; Chen, Q.; Jun, Z. Laser spot center location algorithm of four-quadrant detector based on Gaussian distribution. *Infrared Laser Eng.* **2017**, *46*, 206003. [[CrossRef](#)]
11. Cheng, X.; Yang, Y.; Hao, Q. Analysis of the Effects of Thermal Environment on Optical Systems for Navigation Guidance and Control in Supersonic Aircraft Based on Empirical Equations. *Sensors* **2016**, *16*, 1717. [[CrossRef](#)] [[PubMed](#)]
12. Waldmann, J. Line-of-sight rate estimation and linearizing control of an imaging seeker in a tactical missile guided by proportional navigation. *IEEE Trans. Control Syst. Technol.* **2002**, *10*, 556–567. [[CrossRef](#)]
13. Gapiński, D.; Krzysztofik, I.; Koruba, Z. Analysis of the dynamics and control of the modified optical target seeker used in anti-aircraft rocket missiles. *J. Theor. Applied Mech.* **2014**, *52*, 629–639.
14. Lee, C.H.; Hyun, C.; Lee, J.G.; Choi, J.Y.; Sung, S. A hybrid guidance law for a strapdown seeker to maintain lock-on conditions against high speed targets. *J. Electr. Eng. Technol.* **2013**, *8*, 190–196. [[CrossRef](#)]
15. Fan, J.; An, X.; Lin, P.; Dong, S. A modified biased pursuit guidance for missile with strapdown seeker. In Proceedings of the 2015 Chinese Automation Congress, Wuhan, China, 27–29 November 2015; pp. 1815–1818. doi:10.1109/CAC.2015.7382798. [[CrossRef](#)]
16. Wei, C.Z.; Han, Y.P.; Cui, N.G.; Xu, H.C. Fifth-Degree Cubature Kalman Filter Estimation of Seeker Line-of-Sight Rate Using Augmented-Dimensional Model. *J. Guid. Control Dynam.* **2017**, *40*, 1–8. [[CrossRef](#)]
17. Hartman, R.L.; Griffin, R.W. Faceted Ball Lens for Semi-Active Laser Seeker. U.S. Patent 7,185,845, 6 March 2007.
18. Zhang, J.Q.; Xie, F.; Xue, Q.S.; Xin, J.X. Laser guided lens based on four-quadrant detector. *Chin. Opt.* **2015**, *8*, 471–479. [[CrossRef](#)]
19. Chen, M.; Yang, Y.; Jia, X.; Gao, H. Investigation of positioning algorithm and method for increasing the linear measurement range for four-quadrant detector. *Optik Int. J. Light Electr. Opt.* **2013**, *124*, 6806–6809. [[CrossRef](#)]
20. Wei, Z.; He, Z.; Zhang, X. Optimization design of small optical detection system with large instantaneous field of view. *Infrared Laser Eng.* **2016**, *45*, 518002.
21. Vergez, P.L.; McClendon, J.R. Optimal control and estimation for strapdown seeker guidance of tactical missiles. *J. Guid. Control Dynam.* **1982**, *5*, 225–226, doi:10.2514/3.19767. [[CrossRef](#)]
22. Hyslop, G.; Gerth, D.; Kraemer, J. GPS/INS integration on the standoff land attack missile (SLAM). In Proceedings of the IEEE Symposium on Position Location and Navigation. A Decade of Excellence in the Navigation Sciences, Las Vegas, NV, USA, 20–20 March 1990; pp. 407–412.
23. Chu, H.J.; Tsai, G.J.; Chiang, K.W.; Duong, T.T. GPS/MEMS INS data fusion and map matching in urban areas. *Sensors* **2013**, *13*, 11280–11288. [[CrossRef](#)] [[PubMed](#)]

24. Wu, Y.X.; Wang, J.L.; Hu, D.W. A New Technique for INS/GNSS Attitude and Parameter Estimation Using Online Optimization. *IEEE Trans. Signal Process.* **2014**, *62*, 2642–2655. [[CrossRef](#)]
25. Groves, P.D. *Principles of GNSS, Inertial, and Multisensor Integrated Navigation Systems*; Artech House: Norwood, MA, USA, 2013.
26. Piyabongkarn, D.; Rajamani, R.; Greminger, M. The development of a MEMS gyroscope for absolute angle measurement. *IEEE Trans. Control Syst. Technol.* **2005**, *13*, 185–195. [[CrossRef](#)]
27. Du, S.; Sun, W.; Yang, G. MEMS IMU Error Mitigation Using Rotation Modulation Technique. *Sensors* **2016**, *16*. [[CrossRef](#)] [[PubMed](#)]



© 2018 by the authors. Licensee MDPI, Basel, Switzerland. This article is an open access article distributed under the terms and conditions of the Creative Commons Attribution (CC BY) license (<http://creativecommons.org/licenses/by/4.0/>).